

Ginzburg-Landau model of Bose-Einstein condensation of magnonsB. A. Malomed,¹ O. Dzyapko,² V. E. Demidov,² and S. O. Demokritov²¹*Department of Physical Electronics, School of Electrical Engineering, Tel Aviv University, Tel Aviv 69978, Israel*²*Institute for Applied Physics, University of Münster, 48149 Münster, Germany*

(Received 24 July 2009; published 22 January 2010)

We introduce a system of phenomenological equations for Bose-Einstein condensates of magnons in the one-dimensional setting. The nonlinearly coupled equations, written for amplitudes of the right- and left-traveling waves, combine basic features of the Gross-Pitaevskii and complex Ginzburg-Landau models. They include localized source terms to represent the microwave magnon-pumping field. With the source represented by the δ functions, we find analytical solutions for symmetric localized states of the magnon condensates. We also predict the existence of asymmetric states with unequal amplitudes of the two components. Numerical simulations demonstrate that all analytically found solutions are stable. With the δ -function terms replaced by broader sources, the simulations reveal a transition from the single-peak stationary symmetric states to multi-peak ones, generated by the modulational instability of extended nonlinear-wave patterns. In the simulations, symmetric initial conditions always converge to symmetric stationary patterns. On the other hand, asymmetric inputs may generate nonstationary asymmetric localized solutions, in the form of traveling or standing waves. Comparison with experimental results demonstrates that the phenomenological equations provide for a reasonably good model for the description of the spatiotemporal dynamics of magnon condensates.

DOI: [10.1103/PhysRevB.81.024418](https://doi.org/10.1103/PhysRevB.81.024418)

PACS number(s): 75.40.Gb, 03.75.Nt, 74.20.De

I. INTRODUCTION

The experimental observation of the Bose-Einstein condensation (BEC) in dilute gases of alkali atoms¹ has been a milestone in the development of atomic and condensed-matter physics, demonstrating the reality of this state of matter, and providing a unique testbed for studying numerous macroscopic quantum effects.² As is well known, the transition to the condensation in atomic gases occurs at extremely low temperatures, $\sim 10^{-7}$ K, the number of atoms in the condensate usually being quite small, $\leq 10^4$.

These achievements were followed by the creation of BEC in gases of bosonic quasiparticles representing fundamental excitations in solid-state media, including excitons,³ polaritons,⁴ triplons,⁵ and magnons (spin waves in superfluid phases of ³He (Ref. 6) and in ferromagnets⁷). Similar to the BEC of atomic gases, the condensation of quasiparticles takes place when their density exceeds a certain critical value, which increases with the temperature of the system. However, the advantage of studying BEC in solids is that the density may be increased by external pumping fields: laser or microwave radiation, in the case of excitons and polaritons, or magnons, respectively. Therefore, the BEC transition in solid-state media can be reached at much higher temperatures than in the atomic gases.

Unique properties are featured by the BEC of magnons in tangentially magnetized yttrium-iron-garnet (YIG) films. In particular, the condensation of magnons occurs at room temperatures.^{7,8} Moreover, while, in the first experiments, monochromatic pumping fields were used, it has been recently reported that the BEC of magnons can be achieved by means of an incoherent microwave pumping.⁸

Despite the achievements in the experimental studies of BEC of magnons, development of the corresponding theory is just starting.⁹⁻¹² Thermodynamics of the quasiequilibrium magnon gas and the stability of the condensate were consid-

ered in Refs. 9 and 10, respectively. The formation of the coherent magnon state (the BEC proper), accompanied by the emergence of macroscopic dynamic magnetization, is described in Ref. 11. The theory is capable of explaining, in a quantitative form, the observed intensities of the Brillouin light scattering and microwave signals generated by the condensate. The presented work addresses the dynamics of the magnon condensate, first experimental studies of which were recently reported in Ref. 13.

The magnon BEC is fundamentally different from its counterparts in all other systems. The condensation of magnons occurs at two separate points in the space of the magnon frequency and wave number, $(\omega_0, \pm k_0)$, hence, for the theoretical description of the condensate one needs to introduce wave functions with two components corresponding to these points. One should take into account interactions between these two components, which may result in effects which are not observed in BEC of other (quasi-)particles.

In accordance with the above discussion, different types of models for the description of BEC in atomic gases and solid-state media have to be used. In the former case, a widely adopted theoretical approach is based on the Gross-Pitaevskii equation (GPE) for the single-atom wave function.² In the mean-field approximation, the GPE takes into account collisions between atoms through the cubic term. In fact, the GPE provides for a very accurate model for the practically relevant case of dilute ultracold gases. In condensed matter, GPE and the corresponding Ginzburg-Landau functional have been used for description of different types of magnon BEC in superfluid phases of ³He (Ref. 6). An inherent property of the GPE is that the norm of the wave function is a dynamical invariant, which complies with the obvious condition of the conservation of the number of atoms in the gas. Equations that may serve as a mean-field model of the condensate of quasiparticles should be different, as the quasiparticles (in particular, magnons) may be created by the pump field and lost through linear and nonlin-

ear dissipation. Therefore, the respective equation is expected to be of the complex-Ginzburg-Landau (CGL) type,¹⁴ combining conservative and dissipative terms. However, a difference from the usual form of the CGL equation is that, in the present case, it must include a source term representing the localized pump (in this respect, the equation may be somewhat similar to those describing nonlinear optical cavities pumped by external laser beams¹⁵). Nevertheless, this difference is not absolute, as ultracold atoms have an effective finite lifetime, due to heating effects and three-body interactions. As discussed in Ref. 16, the ratio between the lifetime of the (quasi-)particles and their thermalization time is decisive for this issue. For magnons this factor takes values in the range of 5–10, whereas for ultracold alkali atoms it may reach 2 orders of magnitude.

The objective of the present work is to put forward a semiphenomenological system of coupled equations for the wave functions of the magnon condensate generated by the local microwave source. Comparing predictions of the model with experimental observations of the dynamics reported in Ref. 13, we conclude that the equations correctly reproduce main features of the spatiotemporal dynamics (pattern formation in the condensate). The equations are introduced in Sec. II, and some exact analytical solutions for localized states, predicted by the model, are reported in Sec. III. This is followed by the presentation of numerical solutions in Sec. IV and, eventually by the comparison with the experiment in Sec. V. The paper is concluded by Sec. VI.

II. MODEL

As mentioned above, the onset of the condensation in the magnon gas reveals itself in the emergence of the macroscopic dynamical magnetization in the sample. It should be emphasized that only condensed magnons, with the above-mentioned values of the frequency and wave numbers, $(\omega_0, \pm k_0)$, contribute to this magnetization, whereas all other magnons merely reduce the absolute value of the static magnetization. Following the envelope (slowly varying amplitude) approximation, widely adopted for the analysis of nonlinear spin waves in ferromagnetic films,^{17–19} as well for the description of nonlinear waves in many other settings, we introduce the order parameter (the full wave function of magnons) as

$$\Psi(z, t) = \Psi_+(z, t)e^{ik_0z} + \Psi_-(z, t)e^{-ik_0z}, \quad (1)$$

where absolute values of amplitudes Ψ_{\pm} represent dynamical macroscopic magnetizations created by the corresponding condensate components, m_{\pm} , normalized to the absolute value of the static magnetization (M_0): $|\Psi_{\pm}|^2 = |m_{\pm}|^2 / (2M_0^2)$, while phases of Ψ_{\pm} account for the coherence of the two components of the condensate. In Eq. (1), it is assumed that the magnetic field is aligned with axis z , the microwave antenna is oriented perpendicular to it, and $\pm k_0$ are large wave numbers ($k_0 \approx 3 \times 10^4 \text{ cm}^{-1}$ in YIG films) at which the transition into the BEC state takes place. The remaining dependence on z in $\Psi_{\pm}(z, t)$ is assumed to be slow in comparison with the rapidly oscillating carrier waves, $\exp(\pm ik_0z)$, therefore the interaction between Ψ_+ and Ψ_- is incoherent [see

Eqs. (2) and (3) below]. The slow dependence arises due local variations in the pumping which excites magnons.

In Refs. 17–19 it was shown that, in the case of single-component magnon wave function, the evolution of the envelope is described by the nonlinear Schrödinger equation. In a similar way, for two components Ψ_{\pm} one arrives at a system of phenomenological equations of the GPE/CGL type, which include the above-mentioned source terms, written below as $-f\delta(z)$ to allow analytical treatment of the problem (numerical results will be reported below for a realistic broad shape of the source). In the scaled form, the equations are

$$i(\Psi_+)_t + \delta\mu_0 \cdot \Psi_+ + \frac{1}{2}(\Psi_+)_{zz} + i\eta\Psi_+ + (|\Psi_+|^2 + \sigma_1|\Psi_-|^2)\Psi_+ + i\tau(|\Psi_+|^2 + \sigma_2|\Psi_-|^2)\Psi_+ = -f\delta(z). \quad (2)$$

$$i(\Psi_-)_t + \delta\mu_0 \cdot \Psi_- + \frac{1}{2}(\Psi_-)_{zz} + i\eta\Psi_- + (|\Psi_-|^2 + \sigma_1|\Psi_+|^2)\Psi_- + i\tau(|\Psi_-|^2 + \sigma_2|\Psi_+|^2)\Psi_- = -f\delta(z). \quad (3)$$

Here, $\delta\mu_0$ is a possible shift of the chemical potential of magnons in the condensate with respect to that of uncondensed magnons. We also introduce phenomenological damping, represented by linear and cubic terms in Eqs. (2) and (3), with coefficients η and τ , respectively. The same nonlinear-damping term was introduced in Ref. 20. Further, σ_1 , σ_2 are the XPM/SPM (cross/self-phase-modulation) ratios for the conservative and dissipative nonlinear parts of the equations. The sign in front of the SPM and XPM nonlinearities in the conservative part corresponds to the case of attractive magnon-magnon interaction, which was realized in tangentially magnetized YIG films in experimental works.^{10,19}

It is relevant to mention that equations similar to Eqs. (2) and (3) were derived by Lvov for the description of spatially inhomogeneous parametric excitation of magnons²¹ (in that case, two groups of magnons with wave numbers $\pm k$ were also excited). In fact, the applicability of amplitude equations of this general (*Ginzburg-Landau*) type to the description of condensates is a universal fact (at least, at the phenomenological level), even in the case of strong interactions between quasiparticles.²²

The notation adopted in the equations implies that t is normalized to the characteristic time of the nonlinear interactions of magnons, $\tau_0 \approx 3.6 \text{ ns}$, which, as said above, is much shorter than the lifetime of a magnon [$T_m \approx 250 \text{ ns}$ in YIG (Ref. 23)], hence $\eta \equiv \tau_0 / (2T_m)$ is considered as a small parameter. Spatial coordinate z is normalized to characteristic length z_0 , which is defined by the ratio of the nonlinear interaction strength to the dispersion coefficient [the latter can be calculated from the dispersion relation (Ref. 19) giving $z_0 \approx 0.5 \text{ } \mu\text{m}$ for YIG]. Unlike other coefficients, which may be identified from empirical data, $\delta\mu_0$ should be treated as a phenomenological parameter that may be found from adjusting theoretical predictions to experimental observations.

The strength of the source, f , may be set to be real and positive, by definition. As mentioned above, function $\delta(z)$ in Eqs. (2) and (3) is the Dirac's δ function if we aim to find analytical solutions (see below), or a regularized counterpart of the δ function for numerical solutions. In the latter case, it is taken as

$$\delta(z) \rightarrow \tilde{\delta}(z) \equiv \frac{1}{\sqrt{\pi}\Delta} \exp\left(-\frac{z^2}{\Delta^2}\right), \quad (4)$$

Δ being the regularization parameter.

Note that Eqs. (2) and (3) are somewhat similar to the coupled CGL equations for counterpropagating waves in the binary-fluid thermal convection.²⁴ However, that model includes finite group velocities but not the source terms. Equations (2) and (3) do not contain group-velocity terms [which might be, generally speaking, $\pm ic(\Psi_{\pm})_z$] because the group velocity of magnons vanishes at the condensation points, $k = \pm k_0$.

In the case of the δ function, *symmetric* stationary solutions to Eq. (1) may be sought for as $\Psi_+(z, t) = \Psi_-(z) = \Psi(z)$, where the single complex function, $\Psi(z)$, satisfies an ordinary differential equation,

$$(\delta\mu_0 + i\eta)\Psi + \frac{1}{2} \frac{d^2\Psi}{dz^2} + [(1 + \sigma_1) + i\tau(1 + \sigma_2)]|\Psi|^2\Psi = 0, \quad (5)$$

at $z \neq 0$, supplemented by the boundary condition (bc) at $z = 0$, which is generated by the integration of Eqs. (2) and (3) in an infinitesimal vicinity of $z = 0$,

$$\Psi'|_{z=+0} - \Psi'|_{z=-0} = -2f. \quad (6)$$

The meaning of this bc is that function $\Psi(z)$ must be continuous at $z = 0$ but its derivative makes a jump at the position of the source. This approach to searching for stationary solutions is similar to that which was recently developed for a CGL equation (with an intrinsic gain but without source terms) driven by the deltalike gain.²⁵

Concluding this section, we emphasize that the source term introduced in the above equations is not directly proportional to the microwave field used in the experiment for the parametric pumping of magnons. In fact, the parametric pumping creates primary magnons away from the condensation points in the phase space. The BEC condensate then forms as a result of the thermalization of the primary magnons. Thus, the proposed model does not aim to explicitly describe the spatial spreading of the magnons during the thermalization process.

III. ANALYTICAL RESULTS

A. Symmetric solutions

Following the approach of Ref. 25, where particular exact solutions were found in the framework of the above-mentioned CGL equation with the deltalike linear gain, we look for a localized solution to Eq. (5) in the following form,

$$\Psi(z) = \frac{Ae^{i\chi}}{\{\sinh[\kappa(|z| + \xi)]\}^{1-i\nu}}, \quad (7)$$

with real constants A , χ , κ , ν , and ξ . In particular, ξ must be positive (otherwise, the expression gives rise to a singularity at $|z| = -\xi$). Actually, this *ansatz* was suggested by a formal singular solution to the cubic CGL equation with constant coefficients, that, in turn, is a counterpart to the so-called Pereira-Stenflo soliton, with \sinh replaced by \cosh .²⁶ The latter is a nonsingular but unstable exact solution, which is valid in the case of $\eta < 0$ (a uniform linear gain, instead of the loss). Solutions of the Pereira-Stenflo type may be made stable as exact solutions to coupled CGL equations one of which is cubic and the other one linear.²⁷

The substitution of *ansatz*, Eq. (7), in Eq. (5) leads to the following equations,

$$\kappa^2(2 - \nu^2 - 3i\nu) + 2[(1 + \sigma_1) + i\tau(1 + \sigma_2)]A^2 = 0, \quad (8)$$

$$\kappa^2(1 - i\nu)^2 + 2(\mu_0 + i\eta) = 0. \quad (9)$$

Further, inserting *ansatz*, Eq. (7), into bc, Eq. (6), we arrive at an additional relation,

$$\frac{\cosh(\kappa\xi)}{[\sinh(\kappa\xi)]^{2-i\nu}} = \frac{fe^{-i\chi}}{A\kappa(1 - i\nu)}. \quad (10)$$

Equations (8) and (9) can be solved directly [actually, it is the single physically relevant solution corresponding to *ansatz*, Eq. (7)],

$$\nu = \sqrt{2 + \frac{9(1 + \sigma_1)^2}{4(1 + \sigma_2)^2\tau^2}} + \frac{3(1 + \sigma_1)}{2(1 + \sigma_2)\tau}, \quad (11)$$

$$\kappa^2 = \frac{\eta}{\nu} \equiv \frac{\eta}{2} \left[\sqrt{2 + \frac{(1 + \sigma_1)^2}{(1 + \sigma_2)^2\tau^2}} - \frac{(1 + \sigma_1)}{(1 + \sigma_2)\tau} \right], \quad (12)$$

$$A^2 = \frac{3\eta}{2\tau(1 + \sigma_2)}, \quad (13)$$

$$\delta\mu_0 = \frac{1}{2}(\nu^2 - 1)\kappa^2. \quad (14)$$

It is worthy to emphasize the meaning of Eq. (14): the solution given by *ansatz*, Eq. (7), exists solely for the particular value of $\delta\mu_0$ given by this expression. For other values of $\delta\mu_0$, localized solutions are also expected to exist (see numerical results reported below), but they cannot be found in the exact form corresponding to the present *ansatz*.

Once constants ν , κ , and A are known, as per Eqs. (11)–(13), the equation corresponding to b.c., Eq. (10), can be solved analytically too, and it also produces a single solution, which determines the remaining arbitrary constants, ξ and χ ,

$$\cosh(\kappa\xi) = \sqrt{1 + \frac{A^2\kappa^2(1 + \nu^2)}{4f^2}} + \frac{A\kappa\sqrt{1 + \nu^2}}{2f}, \quad (15)$$

$$\chi = \arctan(\nu) - \nu \ln[\sinh(\kappa\xi)]. \quad (16)$$

A noteworthy feature of solution (15) is the absence of a threshold: any pump strength f , even a very small one, supports the solution. In the limit of $f \rightarrow 0$, Eq. (15) yields $\xi \rightarrow \infty$, which naturally implies the disappearance of the BEC state when the microwave source is switched off.

B. Asymmetric solutions

A challenging issue for the theory is a possibility of the existence of asymmetric solutions with $\Psi_+(z) \neq \Psi_-(z)$. In that case, the stationary version of Eqs. (2) and (3) takes the following form,

$$\begin{aligned} \delta\mu_0 \cdot \Psi_+ + \frac{1}{2}(\Psi_+)_{zz} + i\eta\Psi_+ + (|\Psi_+|^2 + \sigma_1|\Psi_-|^2)\Psi_+ \\ + i\tau(|\Psi_+|^2 + \sigma_2|\Psi_-|^2)\Psi_+ = -f\tilde{\delta}(z), \end{aligned} \quad (17)$$

$$\begin{aligned} \delta\mu_0 \cdot \Psi_- + \frac{1}{2}(\Psi_-)_{yy} + i\eta\Psi_- + (|\Psi_-|^2 + \sigma_1|\Psi_+|^2)\Psi_- \\ + i\tau(|\Psi_-|^2 + \sigma_2|\Psi_+|^2)\Psi_- = -f\tilde{\delta}(z). \end{aligned} \quad (18)$$

Here, we assume that $\tilde{\delta}(z)$ is not an infinitely narrow delta function but rather a regularized one—e.g., as given by Eq. (4). We will demonstrate below that in this case an asymmetric solution appears spatially nonuniformly, i.e., in regions of z , where $\tilde{\delta}(z)$ exceeds a certain threshold.

The possibility of the existence of asymmetric solutions can be investigated analytically under the assumption that the linear and nonlinear dissipative coefficients, η and τ , are large parameters. Strictly speaking, this assumption contradicts the above-mentioned condition for the applicability of the equations to the description of the physically relevant situation, $\eta \ll 1$. Nevertheless, the analysis makes sense, in view of the fundamental significance of the possibility of the symmetry breaking in models of the present type.

Assuming that η and τ are large, in the lowest approximation we neglect all conservative terms and replace Eqs. (17) and (18) by the following ones, for $\Psi_{\pm}(z) \equiv i\Phi_{\pm}(z)$, where functions $\Phi_{\pm}(z)$ are real,

$$\eta\Phi_+ + \tau(\Phi_+^2 + \sigma_2\Phi_-^2)\Phi_+ = f\tilde{\delta}(z), \quad (19)$$

$$\eta\Phi_- + \tau(\Phi_-^2 + \sigma_2\Phi_+^2)\Phi_- = f\tilde{\delta}(z). \quad (20)$$

If an asymmetric solution exists, taking the difference of Eqs. (19) and (20) and dividing it by $\Delta\Phi \equiv \Phi_+ - \Phi_- \neq 0$ yield the following equation,

$$(\sigma_2 - 1)\Phi_+\Phi_- - (\Phi_+^2 + \Phi_-^2) = \eta/\tau. \quad (21)$$

At the *bifurcation point*, where the asymmetric solution splits off from the symmetric one, $\Phi_+ = \Phi_- \equiv \Phi_{\text{symm}}$, Eqs. (19)–(21) must be satisfied simultaneously, i.e.,

$$\eta\Phi_{\text{symm}} + \tau(1 + \sigma_2)\Phi_{\text{symm}}^3 = f\tilde{\delta}(z),$$

$$(\sigma_2 - 3)\Phi_{\text{symm}}^2 = \eta/\tau. \quad (22)$$

The second equation in system, Eq. (22), implies that the bifurcation is only possible if σ_2 is large enough, viz., $\sigma_2 > 3$. Then, the substitution of the second equation into the first one determines the bifurcation point,

$$\Phi_{\text{symm}}^{(\text{bif})} = \frac{(\sigma_2 - 3)}{(\sigma_2 - 1)} \frac{f}{2\eta} \tilde{\delta}(z). \quad (23)$$

Further, equating $\Phi_{\text{symm}}^{(\text{bif})}$, as given by Eq. (23) and by the second equation in system, Eq. (22), yields the value of $\tilde{\delta}(z)$ at the bifurcation point,

$$[f\tilde{\delta}_{\text{bif}}(z)]^2 = \frac{(\sigma_2 - 1)^2 4\eta^3}{(\sigma_2 - 3)^3 \tau f^2}. \quad (24)$$

The meaning of Eq. (24) is that it gives a *threshold condition* for the symmetry-breaking bifurcation. Namely, the bifurcation occurs if the maximum value of $\tilde{\delta}(z)f$, which is its value at the central point, $z=0$ [for instance, $f\tilde{\delta}(0) = f/(\sqrt{\pi}\Delta)$ in the case of $\tilde{\delta}(z)$ given by Eq. (4)] exceeds the threshold value,

$$[f\tilde{\delta}(0)]^2 > [f\tilde{\delta}(0)]_{\text{threshold}}^2 \equiv \frac{(\sigma_2 - 1)^2 4\eta^3}{(\sigma_2 - 3)^3 \tau}. \quad (25)$$

In the present approximation, which corresponds to Eqs. (19) and (20), that do not contain derivatives and therefore admit solutions with discontinuities of the first derivatives, the solution is asymmetric in the region of $|z| < z_{\text{bif}}$, where z_{bif} is to be found from Eq. (24), and the solution continues as the symmetric one to $|z| \geq z_{\text{bif}}$. This structure of the solutions resembles phase-separated states in two-component atomic BEC found from the respective system of coupled GPEs in the Thomas-Fermi approximation.²⁸

IV. NUMERICAL RESULTS

A. Stable symmetric solutions

The numerical analysis was performed by means of direct simulations of Eqs. (2) and (3), using the Crank-Nicolson scheme. Starting with symmetric initial conditions, the simulations of the equations, where the regularized delta function was approximated by Eq. (4) with appropriate values of Δ (in any case, it must be much smaller than the width of the established state), would always drive the solution to a stable symmetric localized state. Varying symmetric initial conditions for fixed parameters of the equations, we always observed the convergence of the numerical solution to the same stationary state, which is clearly an *attractor* of the model—at least, in the class of symmetric initial conditions (see a discussion of asymmetric configurations below).

In all cases when parameter $\delta\mu_0$ was chosen as per Eq. (14), so as to support the existence of the analytical symmetric solution found above, the established state produced by the simulations with $\Delta \leq 1.5$ virtually exactly coincides with the analytically predicted form (thus confirming the *stability* of the analytical solutions). Typical examples are shown in Fig. 1 for two different values of parameter f which accounts for the strength of the pumping. Other constants used for

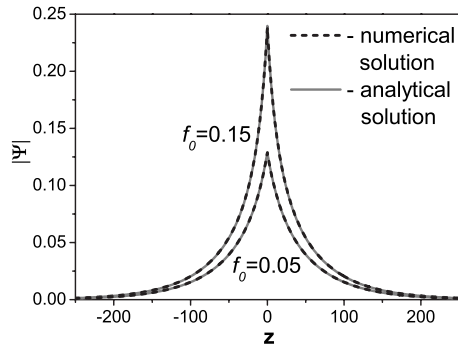


FIG. 1. Analytically predicted and numerically generated profiles of the localized states supported by the δ -function source, at parameter values $\mu_0=0$, $\eta=0.007$, $\tau=0.22$, and $\sigma_1=\sigma_2=2$, $\Delta=1$ for two different values of the source's strength, f (the small value of η used here agrees with the condition of the applicability of the phenomenological model, see the text).

these simulations correspond, after all rescalings, to physical parameters relevant to the experiment (in particular, $\sigma_1=2$ is the value of the XPM/SPM ratio appropriate to the nonlinear wave interactions mediated by the cubic terms²⁹).

Stationary symmetric solutions of another type were produced by the simulations in the case of a broad source, represented by Eq. (4) with much larger values of Δ : the increase in the source's strength, f , and the subsequent growth of the amplitude of the stationary state leads to a transition from the simple localized shape with a single maximum to *multipeak* patterns, as illustrated in Fig. 2. The crossover between the single-peak and multipeak states in the plane of (σ_1, f) , which summarizes results of many simulations performed at different values of the parameters, is displayed in Fig. 3.

In fact, the transition to the multipeak patterns with the increase in the amplitude is a straightforward manifestation of the *modulational instability* of extended states, which is a

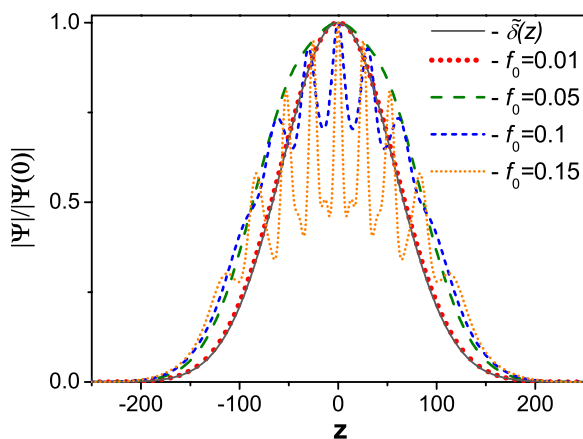


FIG. 2. (Color online) Normalized profiles of stable localized states, obtained with four different values of the strength of the pump, f , in the model with a broad source, corresponding to $\Delta=80$ in Eq. (4). Other parameters are the same as in Fig. 1. Also shown, for comparison, is the shape of the source $\tilde{\delta}(z)$. The transition from the single-peak profile to a multipeak one occurs at some point in interval $0.05 < f < 0.10$.

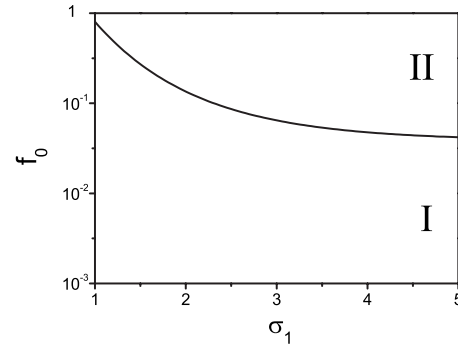


FIG. 3. Stationary localized states generated by the simulations of Eqs. (2) and (3) feature single-peak and multipeak shapes in areas I and II, respectively. Other parameters are $\mu_0=0$, $\eta=0.007$, $\tau=0.22$, and $\sigma_2=3$.

property well known both in conservative models²⁹ and in those based on the CGL equations,¹⁴ provided that the nonlinear terms in the model have the sign corresponding to the self-focusing. As mentioned above, this is indeed the case for the self-interaction of magnons.

B. Asymmetric solutions

The above analysis of the phenomenological model predicted a possibility of the transition from symmetric to asymmetric states, at least in the strongly dissipative system. This possibility was systematically tested by running simulations of Eqs. (2) and (3) with asymmetric initial conditions [in fact, this was done by choosing $\Psi_-(z, t=0)=0$]. We have found that, in some region of the parameter space, any initial condition, symmetric or asymmetric, converges to a single symmetric localized state. On the other hand, another parameter region exists too, where the asymmetric initial configuration generates solutions which remain asymmetric indefi-

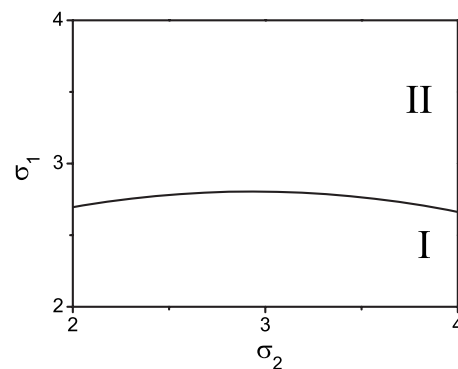


FIG. 4. The border between the areas of (I) monostability and (II) bistability in the plane of parameters (σ_2, σ_1) . Other coefficients are $\mu_0=0$, $\eta=0.007$, $\tau=0.22$, $f=0.15$, and $\Delta=80$. In area II, asymmetric initial conditions, with one component equal to zero, generate persistently asymmetric nonstationary localized solutions, while in area I the same initial conditions converge to stationary symmetric states. In either area, symmetric initial conditions always converge to a stationary symmetric localized state, which may feature a single-peak or multipeak shape in area I, and is always of the multipeak type in area II.

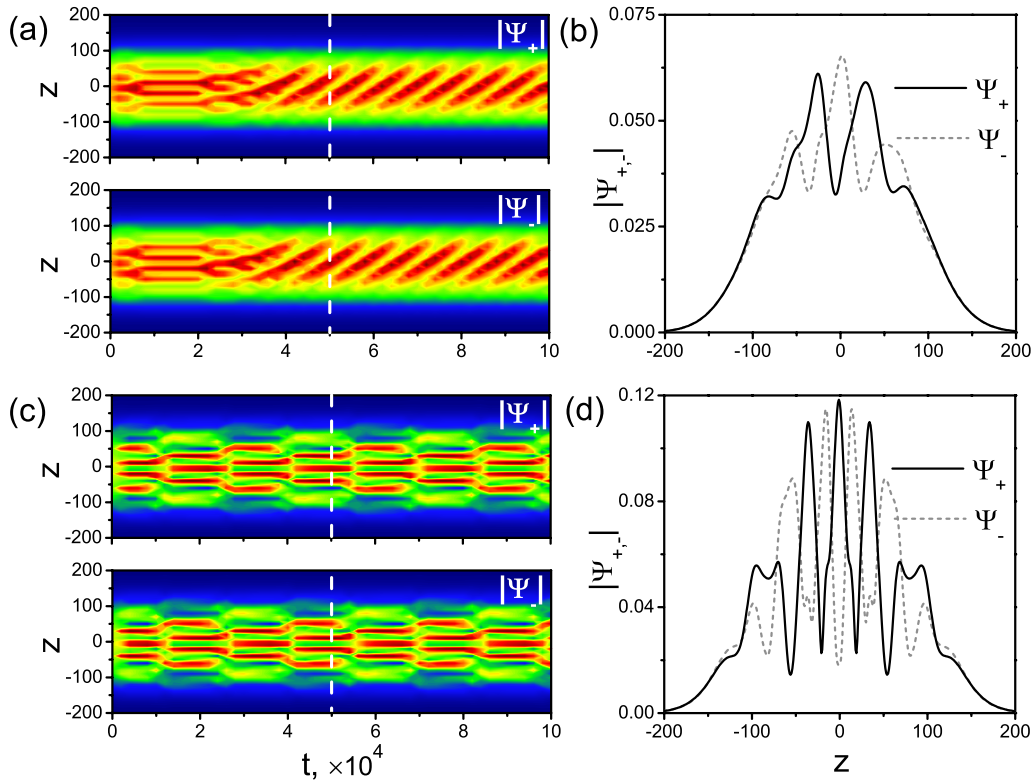


FIG. 5. (Color online) Typical examples of the dynamical behavior of asymmetric states generated by initial conditions with $\Psi_{-}(z, t=0)=0$. Parts (a), (b) and (c), (d) pertain to the pump's strength $f=0.09$ and 0.12 , respectively. Other parameters are $\mu_0=0$, $\eta=0.007$, $\tau=0.22$, $\sigma_1=\sigma_2=3.5$, $\Delta=80$. Panels (a) and (c) display the spatiotemporal evolution of absolute values of the two fields, $|\Psi_{\pm}(z, t)|$, while panels (b) and (d) show the profiles of the solutions observed at $t=50\,000$.

nately long. In fact, this situation implies a *bistability* in the system, as the symmetric input would always generate a stationary symmetric state, at the same values of the parameters. The phase diagram in the parameter space (σ_2, σ_1) showing the regions of the monostability and bistability is displayed in Fig. 4. It is relevant to stress that, with the variation in the parameters, the transition from single-peak to multipeak symmetric states in the class of symmetric solutions (see above) always precedes the onset of the bistability. In other words, in the case of the bistability the symmetric states coexisting with asymmetric ones always represent multipeak patterns.

In fact, the persistently asymmetric states, unlike the symmetric ones, *never* relax to a stationary shape. While keeping an overall localized form, they demonstrate quasiregular oscillations between multi peaked configurations in the two components, Ψ_+ and Ψ_- . Typical examples of the dynamical behavior of asymmetric states are displayed in Fig. 5. It is worthy to note that, at smaller values of the pumping strength, f , each component Ψ_{\pm} of the asymmetric state generates traveling waves, see Fig. 5(a), while at larger values of f the nonstationary dynamics is represented by standing waves, as seen in Fig. 5(c).

In addition to the asymmetry between the components Ψ_+ and Ψ_- , it is relevant to monitor the *spatial* symmetry of these states. The conclusion is that the solutions are spatially asymmetric at lower values of the forcing, $0.07 < f < 0.18$, and they become spatially symmetric, with $\Psi_{\pm}(-z) = \Psi_{\pm}(z)$,

at higher values of f , although the solution remains nonstationary, with unequal components Ψ_+ and Ψ_- . Pairs of panels (a), (c) and (b), (d) in Fig. 5 represent, as a matter of fact, typical examples of the spatial asymmetry and symmetry, respectively (in other words, traveling-wave and standing-wave patterns, as mentioned above).

V. COMPARISON WITH THE EXPERIMENT

The model presented above can be used for the description of recent experiments demonstrating spatiotemporal patterns in magnon condensates formed through the parametric pumping.¹³ The respective pumping field was created by microstrip resonators of two types with different spatial profiles of the microwave field. The spatiotemporal evolution of the condensates was studied using a pumping pulse of a finite width and applying the technique of the time- and space-resolved Brillouin light scattering.

Before comparing the theoretical results with experimental data, it is necessary to stress that the source term in Eqs. (2)–(4), $f\tilde{\delta}(z)$, does not directly represent the pumping field of the resonator used in the experiment. There are two reasons for that. First, in the experiment the resonator excites pairs of primary magnons by means of the parametric pumping. The process of parametric pumping has a threshold with respect to the pumping field. Thus, although, as discussed above, the condensate can be created at any value of f which determines the strength of the source in Eqs. (2) and (3),

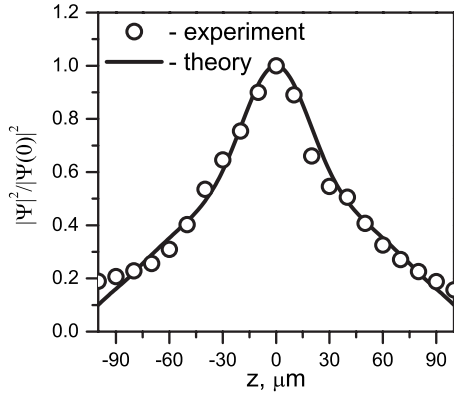


FIG. 6. A typical example of the comparison of the normalized stationary profile of the magnon field, as predicted by the phenomenological equations, and its experimentally observed counterpart. Further details are given in the text.

from the experimental point of view the process has a threshold with respect to the microwave pumping field. Second, the primary magnons create the condensate as a result of the multistep thermalization process,³⁰ which is accompanied by the spreading of the magnon cloud in the physical space. Strictly speaking, to calculate the spatial profile of the pumping, one needs, first, to solve the system of equations similar to Eqs. (2) and (3), which describe the excitation of the primary (parametric) magnons. Then, the so generated profiles should be used in the model accounting for the thermalization process. In its entire form, this problem can hardly be solved even numerically. However, since the group velocity of magnons can be easily found from their spectrum, and the thermalization time is measured experimentally,³⁰ the spreading of the magnon cloud during the thermalization can be estimated as being below 100 μm .

The presence of the effective threshold can be easily taken into account. In Ref. 11 it was shown that the number of magnons in the condensate depends on the strength of the microwave field, h , as $\sqrt{h^2 - h_{\text{thr}}^2}$. Accordingly, we can represent the source term as

$$f\tilde{\delta}(z) \sim \sqrt{h^2(z) - (h_{\text{thr}}^{\text{eff}})^2}, \quad (26)$$

where the effect of the spreading of the magnon cloud during the thermalization process is taken into account by the introduction of the effective threshold field $h_{\text{thr}}^{\text{eff}}$. For values of z at which $h^2(z) - (h_{\text{thr}}^{\text{eff}})^2$ is negative, Eq. (26) is replaced by $\tilde{\delta}(z) = 0$, since no primary magnons are excited in this region.

As mentioned above, the parametric pumping excites pairs of primary magnons with wave numbers $+k_0$ and $-k_0$, which makes experimentally relevant initial conditions for the creation of the condensate symmetric. Therefore, it is not surprising that only symmetric solutions have been observed in the experiment.

For the sake of the qualitative comparison, one needs to determine parameters in Eqs. (2) and (3). The coefficients of the linear and nonlinear dissipation, η and τ , can be extracted from the experimental data via the analysis of the decay of the condensate when the source (pumping field) is switched

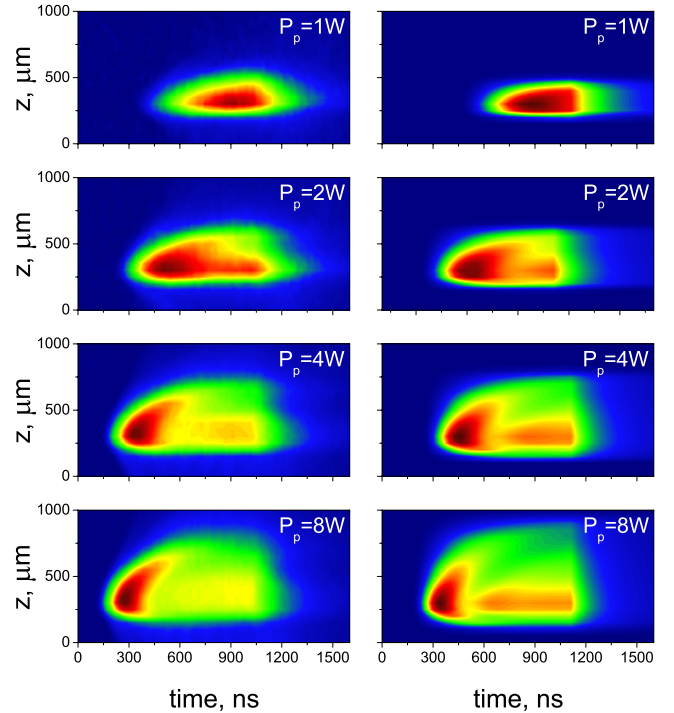


FIG. 7. (Color online) Spatiotemporal evolution of the density of the magnon condensate in the case of the pulsed excitation of the microstrip resonator by the microwave field, for different pumping powers P_p , as indicated in the figure. The left and right columns display the experimental and theoretical results, respectively. Further explanations are given in the text.

off.²³ For the YIG films used in the experiments, these coefficients are found to be $\eta \approx 0.007$ and $\tau \approx 0.22$ (in the scaled notation corresponding to the characteristic nonlinear time of $\tau_0 = 3.6$ ns). Finally, as mentioned above, due to the fact that the nonlinearity in the system is caused by the four-magnon interaction (cubic nonlinearity), the XPM/SPM ratios are $\sigma_1 = \sigma_2 = 2$.

The comparison between the predictions of the phenomenological theory and the experimental data borrowed from Ref. 13 is illustrated in Fig. 6, which shows the spatial profile of the stationary symmetric state calculated using the above parameters and expression (26) for the source. The distribution of the parallel component of the microwave field of the wire resonator was used as $h(z)$, see Fig. 3(a) in Ref. 13. The experimentally measured profile of the condensate density is also shown in Fig. 6. Threshold $h_{\text{thr}}^{\text{eff}}$ in Eq. (26) was treated as a fitting parameter.

Since Eqs. (2) and (3) describe the spatiotemporal dynamics of the condensate, which has been also explored experimentally in Ref. 13, it makes sense to compare spatiotemporal patterns too. Figure 7 represents examples of the spatiotemporal evolution of the magnon field, as predicted by Eqs. (2) and (3), and the respective experimental data. The situation presented in the figure corresponds to the case of the excitation of magnons by the microstrip resonator.¹³ Accordingly, the distribution of the microwave field corresponding to that shown in Fig. 3(b) of Ref. 13 was used for the calculation of the source term, Eq. (26). Point $t=0$ in Fig. 7 corresponds to the start of the pumping pulse. The delay in

the emergence of the condensate is caused by the process of the thermalization of magnons, through their nonlinear interactions, as discussed above.¹³ After about 1000 ns, one observes decay of the condensate density, which is due to the fact that the pumping is switched off at that time. While calculating the theoretical profiles, we have concluded that the most appropriate results are produced by the simulations with $\delta\mu_0 = -0.011$, which corresponds to $-3 \times 10^6 \text{ s}^{-1}$, in the physical units. This value is in agreement with that fact that the pulsed character of the experiment, with characteristic time $t = 1 \text{ }\mu\text{s}$, results in the uncertainty of magnon states within a frequency interval $\Delta f = 2\pi/t \approx 6.28 \times 10^6 \text{ s}^{-1}$.

Comparing the theoretical results and experimental data displayed in Fig. 7, one can conclude that the present model describes the spatiotemporal evolution of magnon condensate fairly well. It is clearly seen that the spatial size of the condensate increases with the growth of the pumping power. This property is explained by the fact that the spatially uniform enhancement of the pumping field, just by increasing the microwave power sent to the resonator, changes the actual profile of the corresponding source. Indeed, for a larger pumping power, condition $h(z) > h_{\text{thr}}^{\text{(eff)}}$, see Eq. (26), is satisfied in a larger interval of z .

VI. CONCLUSION

In this work we have proposed a system of semiphenomenological one-dimensional equations for the dynamical description of the formation of spatiotemporal patterns in Bose-Einstein condensates of magnons. The equations combine essential features of the GPE- and CGL-type models. The equations include localized source terms, which represent the microwave field pumping magnons into the condensate. In

the limit case of the source represented by the δ function, we have found exact analytical solutions for symmetric localized states of the condensate. The model also predicts the possibility of the existence of asymmetric solutions with unequal amplitudes of the left- and right-traveling magnon waves. Systematic simulations of the model have demonstrated that the analytically found solutions are always stable.

Replacing the δ -function source by the broader one, which is relevant to the experimental situation, we have found a transition from the single-peak stationary symmetric solution to stationary multipeak patterns, which may be explained as a manifestation of the modulational instability of broad nonlinear modes. While, in direct simulations, symmetric initial conditions always converge into symmetric stationary states, in a part of the parameter space asymmetric inputs may generate persistently asymmetric nonstationary localized modes, which may be realized as patches of traveling or standing waves, in the cases of low and high amplitudes, respectively.

Comparison with experimental observations demonstrates that the spatial and spatiotemporal patterns predicted by the phenomenological equations may provide for a good model of the experiment, with some parameters found from fundamental characteristics of the ferromagnetic medium, and some others used for the fitting. Moreover, the model suggests to look for new types of patterns in the experiment, such as asymmetric ones.

ACKNOWLEDGMENTS

Support from the Deutsche Forschungsgemeinschaft is gratefully acknowledged. B.A.M. appreciates hospitality of the Institute for Applied Physics at the University of Münster.

-
- ¹M. H. Anderson, J. R. Ensher, M. R. Matthews, C. E. Wieman, and E. A. Cornell, *Science* **269**, 198 (1995); C. C. Bradley, C. A. Sackett, J. J. Tollett, and R. G. Hulet, *Phys. Rev. Lett.* **75**, 1687 (1995); K. B. Davis, M.-O. Mewes, M. R. Andrews, N. J. van Druten, D. S. Durfee, D. M. Kurn, and W. Ketterle, *ibid.* **75**, 3969 (1995).
- ²F. Dalfovo, S. Giorgini, L. P. Pitaevskii, and S. Stringari, *Rev. Mod. Phys.* **71**, 463 (1999).
- ³L. V. Butov, A. L. Ivanov, A. Imamoglu, P. B. Littlewood, A. A. Shashkin, V. T. Dolgoplov, K. L. Campman, and A. C. Gosard, *Phys. Rev. Lett.* **86**, 5608 (2001).
- ⁴J. Kasprzak, M. Richard, S. Kundermann, A. Baas, P. Jeambrun, J. M. J. Keeling, F. M. Marchetti, M. H. Szymaska, R. André, J. L. Staehli, V. Savona, P. B. Littlewood, B. Deveaud, and L. S. Dang, *Nature (London)* **443**, 409 (2006); R. Balili, V. Hartwell, D. Snoke, L. Pfeiffer, and K. West, *Science* **316**, 1007 (2007).
- ⁵T. Giamarchi, C. Rüegg, and O. Tchernyshyov, *Nat. Phys.* **4**, 198 (2008).
- ⁶Yu. M. Bunkov and G. E. Volovik, *J. Low Temp. Phys.* **150**, 135 (2008); G. E. Volovik, *ibid.* **153**, 266 (2008); Yu. M. Bunkov and G. E. Volovik, *J. Phys.: Condens. Matter* (in print), arXiv:0904.3889 (unpublished).
- ⁷S. O. Demokritov, V. E. Demidov, O. Dzyapko, G. A. Melkov, A. A. Serga, B. Hillebrands, and A. N. Slavin, *Nature (London)* **443**, 430 (2006).
- ⁸A. V. Chumak, G. A. Melkov, V. E. Demidov, O. Dzyapko, V. L. Safonov, and S. O. Demokritov, *Phys. Rev. Lett.* **102**, 187205 (2009).
- ⁹A. I. Bugrij and V. M. Loktev, *Low Temp. Phys.* **33**, 37 (2007).
- ¹⁰I. S. Tupitsyn, P. C. E. Stamp, and A. L. Burin, *Phys. Rev. Lett.* **100**, 257202 (2008).
- ¹¹S. M. Rezende, *Phys. Rev. B* **79**, 174411 (2009).
- ¹²S. M. Rezende, *Phys. Rev. B* **80**, 092409 (2009).
- ¹³O. Dzyapko, V. E. Demidov, M. Buchmeier, T. Stockhoff, G. Schmitz, G. A. Melkov, and S. O. Demokritov, *Phys. Rev. B* **80**, 060401(R) (2009).
- ¹⁴I. S. Aranson and L. Kramer, *Rev. Mod. Phys.* **74**, 99 (2002); B. A. Malomed, in *Encyclopedia of Nonlinear Science*, edited by A. Scott (Routledge, New York, 2005), p. 157.
- ¹⁵D. Michaelis, U. Peschel, and F. Lederer, *Phys. Rev. A* **56**, R3366 (1997); L. Spinelli, G. Tissoni, M. Brambilla, F. Prati, and L. A. Lugiato, *ibid.* **58**, 2542 (1998); P. Mandel and M. Tlidi, *J. Opt. B: Quantum Semiclassical Opt.* **6**, R60 (2004); C. O. Weiss and Ye. Larionova, *Rep. Prog. Phys.* **70**, 255 (2007).

- ¹⁶D. Snoko, *Nature (London)* **443**, 403 (2006).
- ¹⁷*Nonlinear Phenomena and Chaos in Magnetic Materials*, edited by P. E. Wigen (World Scientific, Singapore, 1994).
- ¹⁸A. N. Slavin and I. V. Rojdestvenski, *IEEE Trans. Magn.* **30**, 37 (1994).
- ¹⁹A. Zvezdin and A. Popkov, *Sov. Phys. JETP* **57**, 350 (1983).
- ²⁰M. M. Scott and C. E. Patton, *J. Appl. Phys.* **95**, 6294 (2004).
- ²¹V. S. L'vov, *Wave Turbulence under Parametric Excitation* (Springer, Berlin, 1994).
- ²²E. M. Lifshitz and L. P. Pitaevskii, *Statistical Physics, Part 2* (Nauka, Moscow, 1978).
- ²³V. E. Demidov, O. Dzyapko, S. O. Demokritov, G. A. Melkov, and A. N. Slavin, *Phys. Rev. Lett.* **100**, 047205 (2008).
- ²⁴M. C. Cross, *Phys. Rev. A* **38**, 3593 (1988).
- ²⁵C.-K. Lam, B. A. Malomed, K. W. Chow, and P. K. A. Wai, *Eur. Phys. J. Spec. Top.* **173**, 233 (2009).
- ²⁶L. M. Hocking and K. Stewartson, *Proc. R. Soc. London, Ser. A* **326**, 289 (1972); N. R. Pereira and L. Stenflo, *Phys. Fluids* **20**, 1733 (1977).
- ²⁷J. Atai and B. A. Malomed, *Phys. Lett. A* **246**, 412 (1998).
- ²⁸M. Trippenbach, K. Góral, K. Rzażewski, B. Malomed, and Y. B. Band, *J. Phys. B* **33**, 4017 (2000).
- ²⁹Yu. S. Kivshar and G. P. Agrawal, *Optical Solitons: From Fibers to Photonic Crystals* (Academic, San Diego, 2003).
- ³⁰V. E. Demidov, O. Dzyapko, S. O. Demokritov, G. A. Melkov, and A. N. Slavin, *Phys. Rev. Lett.* **99**, 037205 (2007).